https://doi.org/10.1016/j.cej.2021.132832

Metallated terpolymer donors with strongly absorbing iridium complex enables polymer solar cells with 16.71% efficiency

Miao Zhang[a,b], Xiaoling Ma[b,*], Hongyang Zhang[a], Longzhi Zhu[c], Linli Xu[a], Fujun Zhang[b], Chui-Shan Tsang[a], Lawrence Yoon Suk Lee[a], Han Young Woo[d,*], Zhicai He[e,*] and Wai-Yeung Wong[a,c*]

[a] Department of Applied Biology and Chemical Technology and Research Institute for Smart Energy, The Hong Kong Polytechnic University, Hung Hom, Hong Kong, P. R. China

[b] Key Laboratory of Luminescence and Optical Information, Ministry of Education, Beijing Jiaotong University, Beijing 100044, P. R. China

[c] The Hong Kong Polytechnic University Shenzhen Research Institute, Shenzhen 518057, P. R. China

[d] Organic Optoelectronic Materials Laboratory, Department of Chemistry, College of Science, Korea University, Seoul 02841, Republic of Korea

[e] State Key Laboratory of Luminescent Materials and Devices, Institute of Polymer Optoelectronic Materials and Devices, South China University of Technology, Guangzhou, 510640, P. R. China

*** Corresponding author.**

E-mail: maxl@bjtu.edu.cn, hywoo@korea.ac.kr, zhicaihe@scut.edu.cn, wai-yeung.wong@polyu.edu.hk

ABSTRACT

With the sharp growth of non-fullerene acceptors, it is still challenging to develop new polymer donors for highly efficient polymer solar cells (PSCs). Here, a series of metallated terpolymer donors PM6Irx (x = 1%, 3%, 5%) are synthesized by incorporating a new iridium complex, named M1, into the

backbone of the state-of-the-art polymer PM6. The M1 shows a strong absorption in the visible region, which is beneficial to enhance photon harvesting in the active layer. The PM6Ir1:Y6 based PSCs exhibit the best power conversion efficiency (PCE) of 16.71% with short-circuit current density (J_{SC}) of 26.16 mA cm^{-2}, open-circuit voltage (V_{OC}) of 0.848 V and fill factor (FF) of 75.33%. A PCE improvement of about 7% is achieved compared with PM6Ir0:Y6 based control device with PCE of 15.65%, which is due to the markedly increased J_{SC} and FF. The introduction of a moderate amount of M1 enhances the photon harvesting, triplet excitons and lifetime, charge mobility as well as optimizes the active layer morphology. This work indicates that iridium complexes with strong absorption in the visible region have a great potential to promote the photovoltaic performance.

Keywords: polymer donors, terpolymer strategy, iridium complexation, polymer solar cells

1. Introduction

Bulk-heterojunction polymer solar cells (PSCs) have made tremendous advance after more than 20 years of research development in material synthesis, device engineering and mechanistic study. Over the past decades, fullerene and its derivatives ($PC_{61/71}BM$, ICBA) are the most popular electron acceptor materials due to their high electron affinity, high electron mobility and isotropic electron transporting ability. Nevertheless, the highest PCEs of fullerene-based devices are ~12% owing to their limited tunability of energy levels and poor visible light harvesting ability [1-3]. Non-fullerene acceptors can overcome these drawbacks and have received widespread attention since the first report of ITIC by Zhan's group in 2015 [4-6]. Non-fullerene acceptors greatly accelerate the improvement of photovoltaic performance with the advantages of tunable energy levels and strong absorption in the visible and near-infrared regions [7, 8]. The power conversion efficiencies (PCEs) of single-junction PSCs have

exceeded 18%, as summarized in **Table 1**. These highest PSCs are fabricated with the modified non-fullerene acceptors based on the Y6 structure [9]. Because of the complementary advantages of the two kinds of materials, ternary PSCs combining fullerene and non-fullerene as acceptors is an effective strategy to further improve the device performance, which has been proved by many publications [10, 11]. The photoelectric conversion processes are governed by both donor and acceptor components in the bulk-heterojunction system. Developing new polymer donors is equally important to further evaluate the PCEs of non-fullerene acceptors-based PSCs [12]. Terpolymer strategy has been demonstrated as an effective approach to design new conjugated polymer donor or acceptor materials, which comprise three different monomeric units as the repeating groups in the conjugated polymer backbone [13, 14]. Most of the existing terpolymers are designed via the use of three organic monomeric units to obtain the donors or acceptors with better properties [15, 16]. Zhang et al. reported a high-performance terpolymer donor (PM1) by incorporating 20% of the thiophene-thiazolothiazole (TTz) building block into PM6 polymer backbone [17]. The proper introduction of TTz unit enhances the crystallinity and decreases the highest occupied molecular orbital (HOMO) level of the terpolymer, leading to a PCE improvement for PM1:Y6 based PSCs. Guo et al. synthesized a series of terpolymer acceptors (BTI2-xTPD) with bithiophene imide derivatives (f-BTI2) and thienopyrroledione as the acceptor units and 3,4-difluorothiophene as the donor unit [18]. As a result, the PTB7-Th:BTI2-30TPD based all-PSCs can afford an optimal PCE of 8.28%, which was the highest value for the additive-free all-PSCs based on a terpolymer acceptor at that time.

Table 1 Recent progress of highly efficient binary PSCs with PCE over 18%.

Active layer	J_{SC} **(mA cm^{-2})**	V_{OC} **(V)**	**FF (%)**	**PCE (%)**	**Reference**

PM6:L8-BO	26.37	0.89	79.94	18.77	[19]
PM6:L8-BO	26.03	0.893	80.0	18.60	[20]
PM6:EH-HD-4F	27.5	0.84	79.3	18.38	[21]
PM6:L8-BO	25.72	0.87	81.5	18.32	[22]
D18:Y6	27.70	0.859	76.6	18.22	[23]

In addition to the organic monomeric unit, metal complex is also a judicious alternative as the third monomer unit, which contains at least one heavy metal element, such as Pt, Ir, Ru, Zn, Au and so on [18]. The heavy metal centers are in favor of enhancing the intersystem crossing from the lowest singlet to triplet excited states, and thus metal complex can produce more triplet excitons, which is one of their unique strengths compared with most organic materials [24, 25]. The singlet excitons generally have short lifetimes of 10-100 ps and short diffusion lengths of 3-10 nm, which seriously constrain the phase separation and domain sizes of donors and acceptors in the bulk-heterojunction active layer [26, 27]. Triplet excitons have longer lifetimes even up to the order of microseconds due to the forbidden nature of recombination from the triplet states [26]. Metal complexes with long-lived excitons are conducive to reduce geminate recombination and increase free charge generation in the active layer [28, 29]. The introduction of metal complexes provides a novel and feasible idea to fabricate highly efficient PSCs by utilizing the triplet excitons effectively. Recently, it has been demonstrated that metal complexes can modify the molecular aggregation and arrangement in the active layer [30-33]. The molecular regulation may originate from various metal–metal and/or metal–ligand interactions in the active layer. In 2015 and 2020, Huang and Min groups introduced 1% iridium complex, $(dfppy)_2IrdbmBr$, into the polymer conjugated backbone of PTB7 and PM6, respectively [30, 31]. The P1-PTB7Ir1:$PC_{71}BM$ and PM6-

Ir1:Y6 based devices led to a PCE improvement of 45% and 12% compared with the control device, which can be attributed to the enhancement of charge generation and optimization of the active layer morphology. Moreover, in 2017 and 2019, Huang and Peng groups respectively reported two new polymer donors based on the platinum(II) complexation, further illustrating the positive effect of platinum complexes on improving the active layer morphology [32, 33]. To date, related works on using metal complexes for non-fullerene acceptors PSCs are still rare. Typically, most cyclometallated iridium(III) complexes suffer from low absorption coefficients in the visible region and it is necessary to design special ligands to red-shift the absorption profile to the low energy regime (see **Fig. S1**). Organometallic polymer materials have great potential to break through the highest PCE of PSCs by improving the exciton utilization and active layer morphology and at the same time finely tuning the associated energy levels.

Here, we designed and synthesized a series of new polymer donors, as shown in **Fig. 1**, by copolymerizing three monomeric units with different ratios, namely, iridium complex (M1), (4,8-bis(5-(2-ethylhexyl)-4-fluorothiophen-2-yl)benzo[1,2-*b*:4,5-*b*']-dithiophene (BDT-F) and 1,3-bis(thiophen-2-yl)-5,7-bis(2-ethyl-hexyl)benzo-[1,2-*c*:4,5-*c*']dithiophene-4,8-dione (BDD). The monomers BDT-F and BDD were purchased and used as received without further purification. The M1 exhibits a stronger absorption in the visible region compared with other metal complexes reported previously for PSCs, which was synthesized according to the synthetic routes shown in **Fig. S2**. The detailed procedures and characterization are described in **Supporting Information**. The four polymer donors, PM6Ir0, PM6Ir1, PM6Ir3 and PM6Ir5, were obtained by incorporating 0%, 1%, 3% and 5% M1 into the conjugated polymer backbone. The PM6Ir0 as the reference is a superior donor material, which has been widely reported in highly efficient PSCs [34, 35]. The introduction of M1 could be propitious to produce more

triplet excitons with a long lifetime in the active layer due to the presence of triplet-based iridium component. Free charge generation would be greatly improved in the active layer for producing a higher short-circuit current density (J_{SC}) if triplet excitons can be accessed effectively. The introduction of M1 enhances the absorption intensity of polymer donors in the visible region and slightly adjusts the energy levels of the polymer donors. The PM6Ir1:Y6 based PSCs exhibit the highest PCE of 16.71% with a J_{SC} of 26.16 mA cm^{-2}, open-circuit voltage (V_{OC}) of 0.848 V and fill factor (FF) of 75.33%. A PCE improvement of about 7% is achieved compared with the PM6Ir0:Y6 based control device with a PCE of 15.65%. The photon harvesting ability and charge mobility of the active layer are markedly enhanced, which is the major reason for the increase of J_{SC} in the optimized PSCs. The positive effect of M1 on the active layer morphology and molecular arrangement is confirmed, which is in favor of reducing the charge carrier recombination for the increased FF of the optimal PSCs. The triple exciton dynamic processes would be the key and challenging issues to address for organometallic polymer donor materials, especially those with only a tiny proportion of the metal complex.

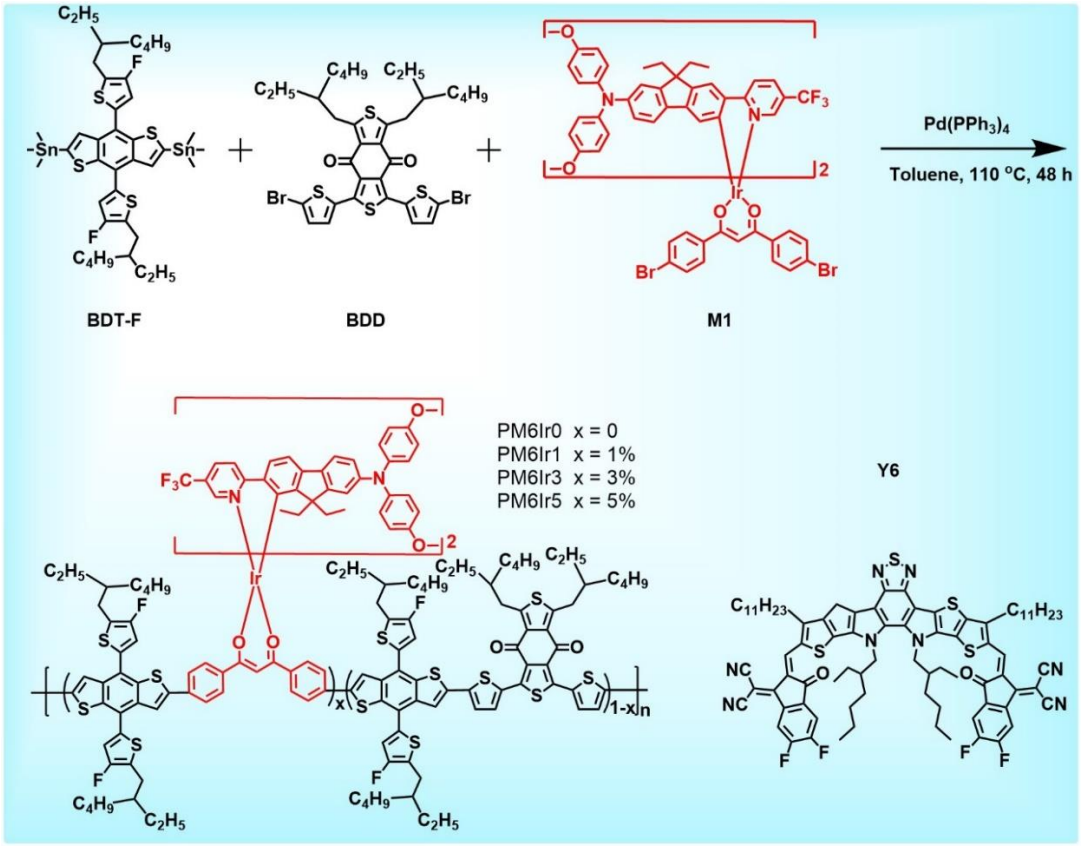

Fig. 1. Synthetic routes of new polymer donors and chemical structures of the used materials.

2. Results and discussion

All polymer donors are produced by the Stille coupling type copolymerization of three monomers, BDT-F, BDD and M1 (**Fig. 1**) [36]. The molar ratio of BDT-F to (BDD+M1) remains 1:1 for all polymer donors, and only the M1/BDD ratio is adjusted to afford four different polymer donors, PM6Ir0, PM6Ir1, PM6Ir3 and PM6Ir5. The detailed synthetic method of polymer donors is described in **Supporting Information**. The inductively coupled plasma mass-spectrometry (ICP-MS) measurement using an Agilent Technologies 7900 ICP-MS instrument was carried out to further identify the content of iridium component, as shown in **Fig. 2a**. The HNO_3/H_2SO_4 blend solution is selected as the digestion system for the four polymers. According to the perfect linear fit of iridium standard signals with the coefficient of determination R^2 = 1.0, the measured concentration of iridium component is 0.022 ppb, 1.093 ppb,

4.099 ppb and 9.620 ppb for PM6Ir0, PM6Ir1, PM6Ir3 and PM6Ir5, respectively. The results well demonstrate that the content of iridium component is gradually increased along with the increase of M1 concentration in the feed ratio, which is firstly reported in this work. It is difficult to use the calculated concentration to represent the actual percentage of iridium component due to the uncertain degree of polymerization and dispersion as well as the inevitable loss of iridium from the filtration process. Moreover, all polymer donors can be reasonably dissolved in chloroform, which is the prerequisite for device fabrication and material characterization. According to the gel permeation chromatography (GPC) measurement, the number average molecular weights (M_n) are 30.8 kDa, 29.8 kDa, 37.6 kDa, 47.7 kDa for PM6Ir0, PM6Ir1, PM6Ir3, PM6Ir5 and the corresponding polydispersity indexes (PDI) are 1.51, 1.48, 1.96, 2.62, respectively. In the thermogravimetric analysis (TGA) measurement using Mettler Toledo TGA/DSC 3+ system, the decomposition temperatures (T_d) of the four polymer donors are 433 ℃, 437 ℃, 441 ℃ and 437 ℃ when its weight is reduced to 95% of the initial value in each case, as shown in **Fig. 2b**. So, the thermal stability of polymer donors is slightly improved through the introduction of M1 into the polymer backbone. Based on the high T_d values of the polymers, it is feasible for the active layer to be subject to thermal annealing treatment at 100 ℃. **Fig. S3a** shows the absorption spectrum of iridium complex **M1** in dichloromethane solution. Compared with most of the reported iridium complexes (**Fig. S1**), M1 displays a stronger absorption in the visible region with a higher absorption coefficient (ε = 6.2 × 10^4 M^{-1} cm^{-1}) at 444 nm. The normalized absorption spectra of M1, polymer donors and Y6 acceptor in the film state were investigated, which are depicted in **Fig. 2c**. The absorption range and peak location do not change much for the four polymer donors. It can be observed that the absorption intensity of the polymer donors is enhanced in the 300-600 nm region along with the increase of M1 content. Absorption coefficient of the pristine polymer was measured in chloroform

solution, as depicted in **Fig. S3b** (the measurement concentration of the polymer solution is 1×10^{-3} g/L). The weight but not molar concentration of polymer solution is used to calculate the corresponding absorption coefficient due to the uncertain molar weight of the polymers. The absorption coefficient of polymer solution is increased with the growth of M1 content in the wavelength range from 350 nm to 600 nm, which is consistent with the result of the polymer films. These polymer donors and Y6 acceptor exhibit complementary absorption in the whole wavelength range, which is beneficial to the photon harvesting in the active layer. **Fig. 2d** portrays the cyclic voltammetry (CV) curves of the polymer donors in films. The highest occupied molecular orbital (HOMO) and the lowest unoccupied molecular orbital (LUMO) levels are slightly decreased upon introducing M1 into the polymer backbone. The energy levels of these polymers match well with the acceptor Y6 (HOMO/LUMO = -5.65/-4.10 eV) for efficient exciton dissociation [37]. **Table S1** summarizes the related optoelectronic parameters of the polymer donors.

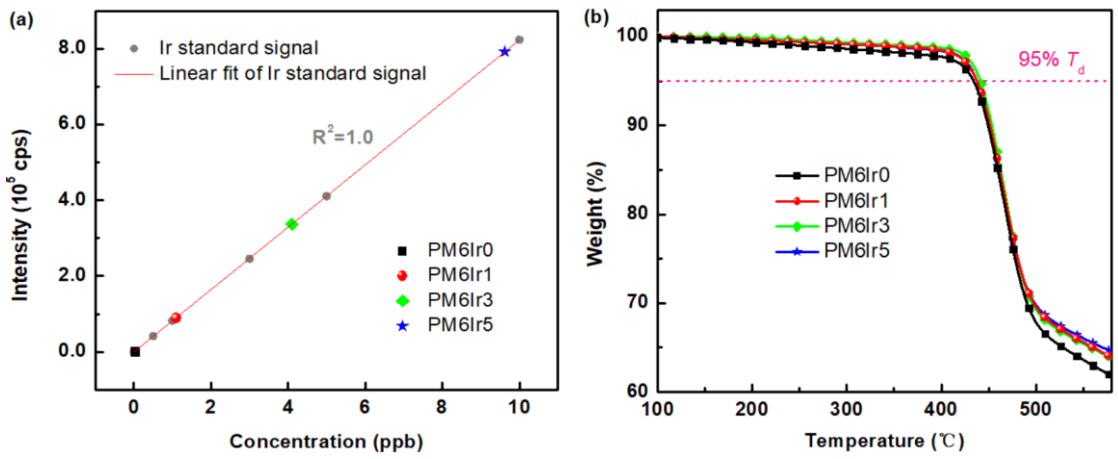

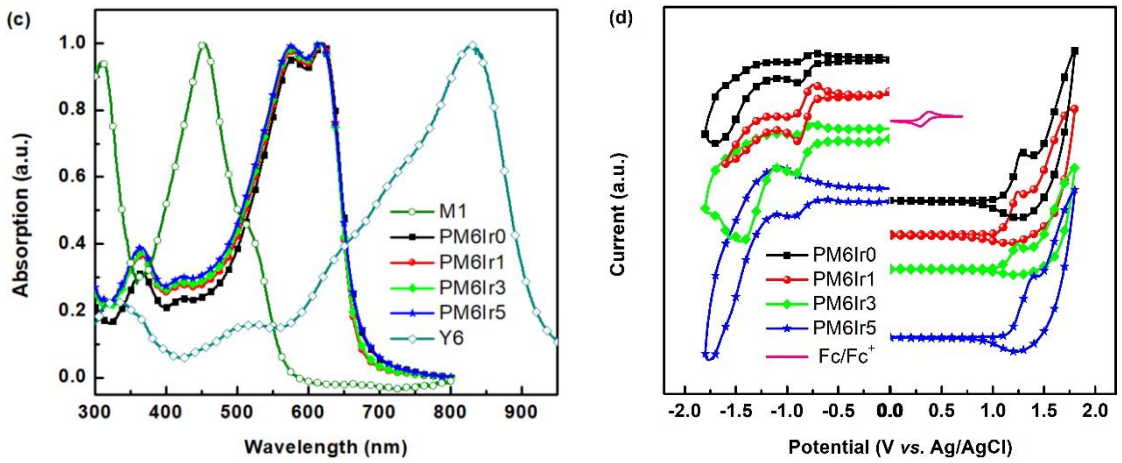

Fig. 2. (a) Linearly fitted ICP-MS curves of iridium standard and polymer signals; (b) TGA plots of polymer donors with a heating rate of 10 ℃ min^{-1} under a N_2 atmosphere. (c) Normalized absorption spectra of M1, polymers and Y6 in films; (d) CV curves of polymers in films.

In order to explore the influence of M1 content on the photovoltaic performance, PM6Irx:Y6 (x = 0, 1%, 3%, 5%) based PSCs were fabricated with the architecture of ITO/PEDOT:PSS/active layer/PDIN/Al under the same conditions. Current density-voltage (*J*-*V*) curves of all PSCs are presented in **Fig. 3a** and the key photovoltaic parameters are summarized in **Table 2**. The PM6Ir0:Y6 based control device reveals a PCE of 15.65% with a J_{SC} of 25.21 mA cm^{-2}, V_{OC} of 0.842 V and FF of 73.71%. The four parameters of the control device are comparable to the values in many literature reports, demonstrating the reliability of our experimental results [38-40]. Compared with the control device, the J_{SC} values of PM6Irx based devices show a marked increase which reaches over 26 mA cm^{-2} for PM6Ir1:Y6 and PM6Ir3:Y6 based PSCs. The FF values of PM6Irx based PSCs are firstly improved and then decreased as the M1 content varies from 1% to 3%. The optimal PCE of 16.71% is achieved for PM6Ir1:Y6 based PSCs with a J_{SC} of 26.16 mA cm^{-2}, V_{OC} of 0.848 V and FF of 75.33% based on the common solvent of chloroform, additive of 1-chloronaphthalene and anode/cathode interlayer of

PEDOT:PSS/PDIN. **Table S2** summarizes the photovoltaic parameters of some representative binary PSCs with PM6:Y6 as the active layer undergoing different treatments. The PCEs of the most optimal PSCs are between 16% and 17% by optimizing the solvent used, additive and anode/cathode interlayer. Compared to polymer cathode interlayer, PNDIT-F3N, used by Min's group [25], the PCE of 16.71% in this work is obtained based on a cheaper small-molecule cathode interlayer, PDIN, which is easier to purify and has a better batch-to-batch reproducibility. The V_{OC} values of all PSCs are kept at ~0.84 V, which is consistent with the HOMO results of the four polymer donors. For PM6Ir5:Y6 based PSCs, the J_{SC} and FF values go down to 25.09 mA cm^{-2} and 70.91%, leading to a relatively low PCE of 14.97%. The decreased PCE should be attributed to the destructed bi-continuous interpenetrating network in the active layer when introducing an excessive dose of M1 into the polymer backbone. The compatibility among the metal complex and the other two organic monomers is a critical ingredient for developing highly efficient organometallic polymer donor materials, which need a continuous exploration on their molecular design. To further confirm the effect of M1 content on the photovoltaic performance, **Table 2** lists the average PCE and standard deviations for all PSCs based on 15 devices from different batches. All *J-V* curves of the control and optimal devices are shown in **Fig. S5** and the detailed photovoltaic parameters are listed in **Table S3-S4**. The positive effect of M1 on the PCE improvement can be intuitively observed from **Fig. 3b**. The optimal device yields a PCE improvement of about 7% compared with the control device. We also fabricated PSCs with PM6Ir1:N3 and PM6Ir1:ITIC-Th as the active layers. The chemical structures of the used materials and schematic diagram of PSCs are shown in **Fig. S6** and photovoltaic parameters of the corresponding PSCs are listed in **Table S5**. The PM6Ir1:N3 and PM6Ir1:ITIC-Th based PSCs exhibit good performance with PCE of 16.27% and 10.39%, respectively. The optimal polymer PM6Ir1 can work well with three non-fullerene acceptors.

The external quantum efficiency (EQE) versus wavelength spectra of all PSCs were measured and displayed in **Fig. 3c** to better explain the variation of J_{SC} in different cases. All PSCs exhibit a broad EQE spectral range from 300 to 950 nm. The relatively low EQE is observed for the control device in the range from 700 to 950 nm. The EQE is markedly increased in the long wavelength range from 500 to 950 nm for PM6Ir1:Y6 and PM6Ir3:Y6 based PSCs. The optimal PSCs exhibit a higher and flatter EQE spectrum in the whole wavelength range, resulting in the highest J_{SC} of 26.16 mA cm^{-2} for PM6Ir1:Y6 based PSCs. The calculated J_{SC} values according to the EQE spectra are 24.30 mA cm^{-2}, 25.13 mA cm^{-2}, 24.81 mA cm^{-2} and 23.97 mA cm^{-2}, respectively, for PM6Ir0/PM6Ir1/PM6Ir3/PM6Ir5:Y6 based PSCs. The calculated values match well with the experimental values from the *J-V* curves with an acceptable mismatch below 5%. The photon harvesting strength in the short wavelength range should be enhanced according to the absorption spectra of the neat polymer films, which is one of the reasons for the EQE improvement of the corresponding PSCs. The transmittance spectrum of PEDOT:PSS/ITO film in **Fig. S4** indicates that the solar light region beyond 400 nm can be mainly utilized in PSCs. As seen from the ΔEQE spectra (the difference between EQE value of the PM6Ir0:Y6 based and PM6Irx (x=0, 1, 3, 5):Y6 based PSCs) in **Fig. S4**, the EQE values from 400 nm to 900 nm are higher for PM6Ir1/PM6Ir3:Y6 based PSCs than that of PM6Ir0:Y6 based PSCs. The increased EQE values of PSCs in the whole wavelength range are attributed to the synergistic effects of the enhanced absorption intensity as well as the optimized charge transport and collection in the active layers [41]. The results suggest that the introduction of M1 shows a palpable improvement on J_{SC} of PSCs.

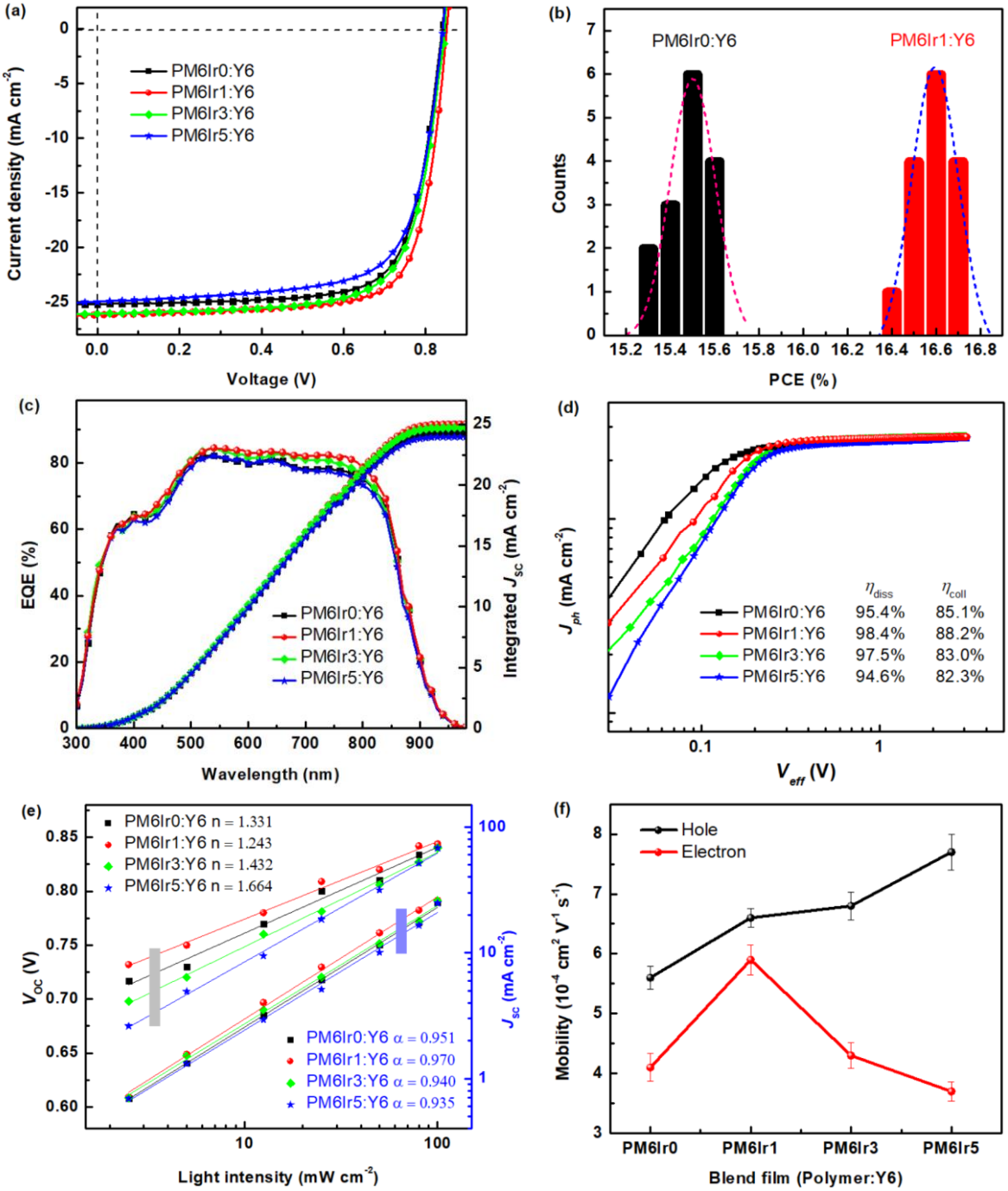

Fig. 3. (a) *J*-*V* curves of all PSCs; (b) PCE distribution of PM6Ir0:Y6 and PM6Ir1:Y6 based PSCs from 15 devices; (c) EQE spectra of all PSCs; (d) J_{ph}-V_{eff} curves of all PSCs; (e) J_{SC}-P_{light} and V_{OC}-P_{light} curves of all PSCs; (f) Hole and electron mobilities of polymer:Y6 films.

Table 2 Photovoltaic parameters of all PSCs.

Device	J_{SC}	Calc. J_{SC}	V_{OC}	FF	PCE

	(mA cm^{-2})	(mA cm^{-2})	(V)	(%)	(%)
PM6Ir0:Y6	25.21	24.30	0.842	73.71	15.65 (15.51±0.10)
PM6Ir1:Y6	26.16	25.13	0.848	75.33	16.71 (16.60±0.08)
PM6Ir3:Y6	26.08	24.81	0.843	72.81	16.01 (15.85±0.15)
PM6Ir5:Y6	25.09	23.97	0.841	70.93	14.97 (14.77±0.17)

Calc. J_{SC} is the J_{SC} value of PSCs calculated from the corresponding EQE spectra.

The photocurrent density *vs* effective voltage (J_{ph}-V_{eff}) characteristics were employed to study the exciton dissociation and charge collection process in the active layer, as depicted in **Fig. 3d**. Here, J_{ph} value is equal to the current density difference under illumination and dark conditions. V_{eff} value is equal to the difference between V_0 and the applied voltage, in which V_0 represents the voltage at J_{ph} = 0. The saturation current density (J_{sat}) is defined as the J_{ph} at a relatively high V_{eff} of 3.0 V. The exciton dissociation efficiency (η_{diss}) and charge collection efficiency (η_{coll}) can be evaluated by the J_{ph}/J_{sat} values under short-circuit and the maximum power output conditions [42, 43]. The calculated η_{diss}/η_{coll} values are 95.4%/84.1%, 98.4%/88.2%, 97.5%/83.0% and 94.6%/82.3% for PM6Ir0/PM6Ir1/PM6Ir3/PM6Ir5:Y6 based PSCs, respectively. The highest η_{diss} and η_{coll} values suggest that the exciton dissociation and charge collection process are optimized in PM6Ir1:Y6 based active layer, giving more evidence on the J_{SC} and FF enhancement for the optimal device. **Fig. 3e** exhibits the dependence of J_{SC} and V_{OC} on light intensity (P_{light}) of all PSCs to explore the charge recombination in the active layer. The detailed *J*-*V* curves under different light intensities are shown in **Fig. S7**. The J_{SC}-P_{light} and V_{OC}-P_{light} curves were fitted according to the formulas of $J_{SC} \propto P_{light}^{\alpha}$ and $V_{OC} \propto n(\kappa T/q)\ln P_{light}$, where κ is the Boltzmann's constant, T is the absolute temperature, and q is the

elementary charge [44]. Compared with PM6Ir0:Y6 based PSCs, the α value is increased from 0.951 to 0.970, while n value is decreased from 1.331 to 1.243 for PM6Ir1:Y6 based PSCs. Both bimolecular and trap-assisted recombination should be suppressed in the PM6Ir1:Y6 based active layer, which is beneficial to the increase of J_{SC} and FF [45]. The charge recombination becomes more serious according to the decreased α value of 0.935 together with the increased n value of 1.664 for PM6Ir5:Y6 based PSCs, leading to the decreased device performance. The increased charge recombination might be attributed to the poorer active layer morphology after introducing an excess quantity of M1 into the polymer backbone.

The charge mobility was investigated by the space-charge-limited current (SCLC) model, which can make the effect of M1 introduction on the charge transport in the active layer more clear [46, 47]. The hole-only and electron-only devices were fabricated with the structures of ITO/PEDOT:PSS/active layer/MoO_3/Ag and ITO/ZnO/active layer/PDIN/Al, respectively. The current-voltage characteristics of the hole-only and electron-only devices were measured in dark and the corresponding $\ln(Jd^3 V^{-2})$-$(V d^{-1})^{0.5}$ curves are plotted in **Fig. S8**. The hole and electron mobilities are calculated according to the Mott-Gurney equation with the Poole-Frenkel correction, as described in **Supporting Information**. The hole mobilities are 5.6×10^{-4}, 6.6×10^{-4}, 6.8×10^{-4} and 7.7×10^{-4} $cm^2\ V^{-1}\ s^{-1}$ and electron mobilities are 4.1×10^{-4}, 5.9×10^{-4}, 4.3×10^{-4} and 3.7×10^{-4} $cm^2\ V^{-1}\ s^{-1}$ for PM6Ir0/PM6Ir1/PM6Ir3/PM6Ir5:Y6 based blend films, respectively. **Fig. 3f** shows a line graph of the hole and electron mobilities from all blend films. Compared with the PM6Ir0:Y6 based blend films, the hole mobility is gradually increased by introducing M1 into the polymer backbone. The molecular crystallinity and packing should be improved in the M1-containing blend films, leading to the increased hole mobility [48]. The introduction of M1 is beneficial to hole transport in the active layers, which is further demonstrated by the increased hole

mobilities of the M1-containing polymer films, as shown in **Fig. S9**. The electron mobility is increased and then decreased along with the growth of the M1 content in blend films. The obviously decreased electron mobility for the PM6Ir5:Y6 blend films could be ascribed to the relatively discontinuous electron transport pathway due to more isolated Y6 domains caused by the excessive aggregation of PM6Ir5, as disclosed below [31, 49]. The trend of the hole and electron mobilities is similar to that reported by others [50]. The significantly increased hole and electron mobilities were obtained for PM6Ir1:Y6 based blend films, which is conducive to the charge extraction in the active layer for causing a higher J_{SC}. The ratio of hole and electron mobilities (μ_h/μ_e) reaches 1.2 for PM6Ir1:Y6 based blend films, which is closest to 1 compared with the values from the rest of the blend films. The results indicate that a quicker and more balanced charge transport should be achieved in the active layer, thus contributing to the simultaneously increased J_{SC} and FF for the PM6Ir1:Y6 based PSCs [51, 52]. Compared with the μ_h/μ_e value of 1.4 for PM6Ir0:Y6 based blend films, the relatively large μ_h/μ_e of 2.1 was acquired for PM6Ir5:Y6 based blend films, which could result in the unbalanced charge transport in the corresponding active layer, and thus considerably reduced FF.

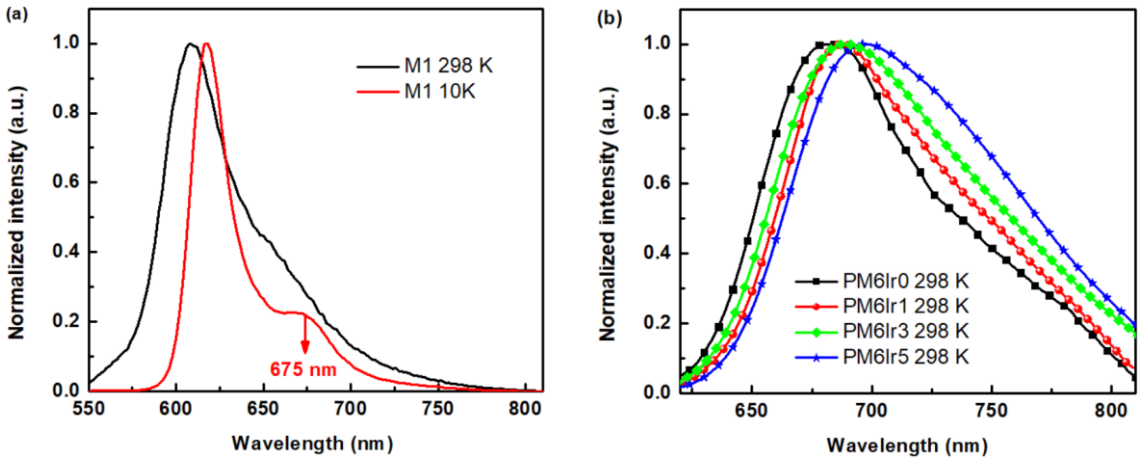

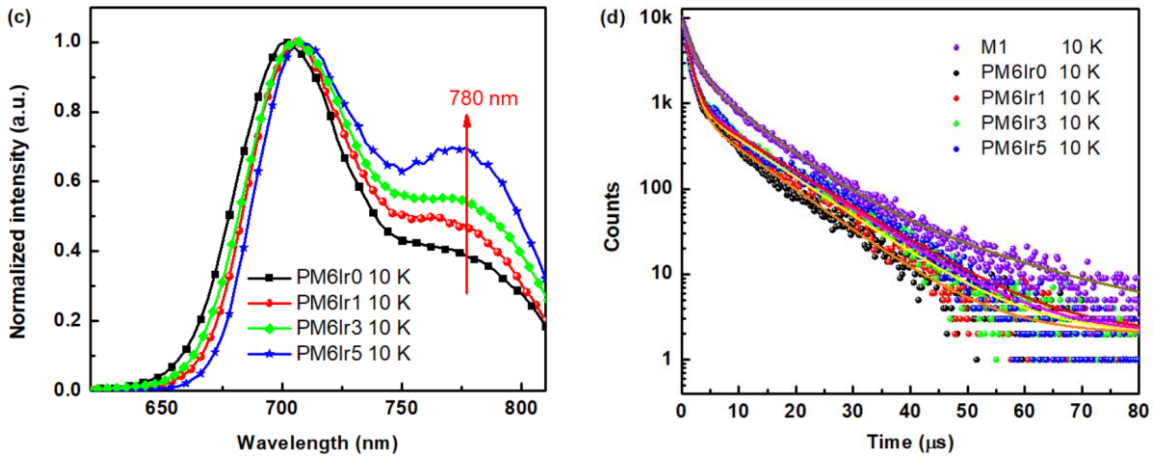

Fig. 4. (a) PL spectra of M1 film at 298 K and 10 K; (b) PL spectra of polymer films at 298 K; (c) PL spectra of polymer films at 10 K; (d) T_1-decayed curves for M1 film probing 675 nm light emission and polymer films probing 780 nm light emission at 10 K.

Table 3 The fitted lifetime parameters for M1 and polymer films.

Lifetime	τ_1 (μs)	τ_2 (μs)	τ_3 (μs)	A_1	A_2	A_3	$<\tau>$ (μs)
M1	1.62	7.58	21.04	6649.7	2588.4	185.7	7.24
PM6Ir0	1.15	8.95	-	9072.6	900.8	-	4.55
PM6Ir1	1.08	9.57	-	9092.1	1083.8	-	5.44
PM6Ir3	1.09	9.85	-	8906.7	1184.8	-	5.87
PM6Ir5	1.15	10.47	-	9030.9	1064.8	-	5.98

$$<\tau> = (A_1{\tau_1}^2 + A_2{\tau_2}^2 + A_3{\tau_3}^2)/(A_1\tau_1 + A_2\tau_2 + A_3\tau_3)$$

The steady-state and transient photoluminescence (PL) spectral measurements were executed to monitor the triplet-exciton signals from M1 and polymer films. **Fig. 4a** displays the normalized PL spectra of M1 film at 298 K and 10 K. The M1 film at 298 K exhibits the broad emission ranging from 550 nm to 800 nm with a PL peak at 610 nm, which can be assigned to the triplet state (T_1) to the ground state (S_0) phosphorescence emission due to the metal-to-ligand charge transfer (MLCT) characteristics

[53, 54]. The PL peak is red-shifted to 615 nm for M1 film at 10 K with a new vibronic sub-band peak at 675 nm. The normalized PL spectra of polymer films (PM6Ir0/PM6Ir1/PM6Ir3/PM6Ir5) were further recorded at 298 K and 10 K, as displayed in **Fig. 4b** and **4c**. The PL peak positions of four polymer films have the same red-shifted trend as the M1 film when the text temperature drops from 298 K to 10 K. There is a new PL peak at 780 nm for the polymer films at 10 K, originating from the emission of the triplet excitons of the polymer films. There is a better vibronic fine transition for polymer films due to the suppression of thermally activated nonradiative decay at a low temperature [55]. The PL peak intensity is gradually increased along with the growth of M1 feed ratio, suggesting that the introduction of M1 is conducive to generate more triplet excitons in the polymer films. The T_1-decayed curves at 10 K was monitored under 675 nm for M1 film and 780 nm for the polymer films, as shown in **Fig. 4d**. The curves were fitted and the corresponding lifetime data are enumerated in **Table 3**. The average lifetime $<\tau>$ was calculated by the following formula:

$$<\tau> = \frac{A_1{\tau_1}^2 + A_2{\tau_2}^2 + A_3{\tau_3}^2}{A_1\tau_1 + A_2\tau_2 + A_3\tau_3}$$

The M1 exhibited the longest T_1-decayed lifetime $<\tau>$ of 7.24 μs due to strong MLCT characteristic. The T_1-decayed lifetime $<\tau>$ is monotonically increased from 4.55 μs to 5.98 μs for PM6Ir0, PM6Ir1, PM6Ir3 and PM6Ir5 films. The polymer PM6Ir50 with M1/BDD ratio of 1:1 was synthesized to further confirm the experimental results. **Fig. S10a** shows the normalized absorption and PL spectra of PM6Ir50 film at 298 K and 10 K. The absorption intensity is evidently enhanced in the range from 300 nm to 500 nm due to the increased M1 content. The main PL peak is located at 660 nm at 298 K and 682 nm at 10 K for PM6Ir50 film. The triplet-state PL peak is blue-shifted to 750 nm for PM6Ir50 film at 10 K and the T_1-decayed lifetime $<\tau>$ reaches 5.43 μs shown in **Fig. S10b**. Compared with the PM6Ir0 film, the triplet-state PL peak intensity and T_1-decayed lifetime are not obviously enhanced along with the large

increase of M1 content, which should be mainly derived from the organic monomers in the polymer backbone. The separate PL signal from M1 is not observed for all polymer films whether at 298 K or 10 K, which should overlap with that of the organic monomers, even though with large M1 content. The T_1 energy levels of the polymer films play a vital role for the utilization of triplet excitons, which directly determines the exciton dissociation process at the polymer/Y6 interfaces. **Fig. S10c** depicts the absorption and PL spectra of the polymer films to calculate the S_1 energy level through the crossing points of both spectra [56]. The polymer films exhibit similar $E(S_1)$ values of about 1.895-1.905 eV, which matches well with the CV results. As illustrated in **Fig. 4c**, the polymer films at 10 K show the phosphorescent emission peaks at 780 nm, corresponding to an $E(T_1)$ of 1.589 eV [57]. For organic solar cells, the charge transfer state E(CT) is usually obtained according to the Marcus theory by fitting the low-energy shoulder of the electroluminescence spectra and Fourier-transform photocurrent spectroscopy external quantum efficiency spectra [58]. The E(CT) of 1.342 eV for the PM6/Y6 system has already been investigated [59]. Owing to the small energy offset of about 0.29 eV or 0.30 eV between $E(T_1)$ and E(CT), Huang et al. concluded that the triplet excitons from H1 or H2 acceptors may provide sufficient time to subsequently dissociate excitons into free charges and thus contribute to photovoltaic performance of the PBDB-T:H1 and PBDB-T:H2 based devices [29]. They also came up with the same conclusion in the D18:BT3-4Cl-based system [60]. **Fig. S10d** schematically shows some key energy levels in the active layer. The energy offset of about 0.247 eV between $E(T_1)$ and E(CT) might be beneficial to the triplet exciton dissociation. Therefore, the increased triplet excitons as well as exciton lifetime of the polymer films should be advantageous to the device performance improvement, especially, the J_{SC} value.

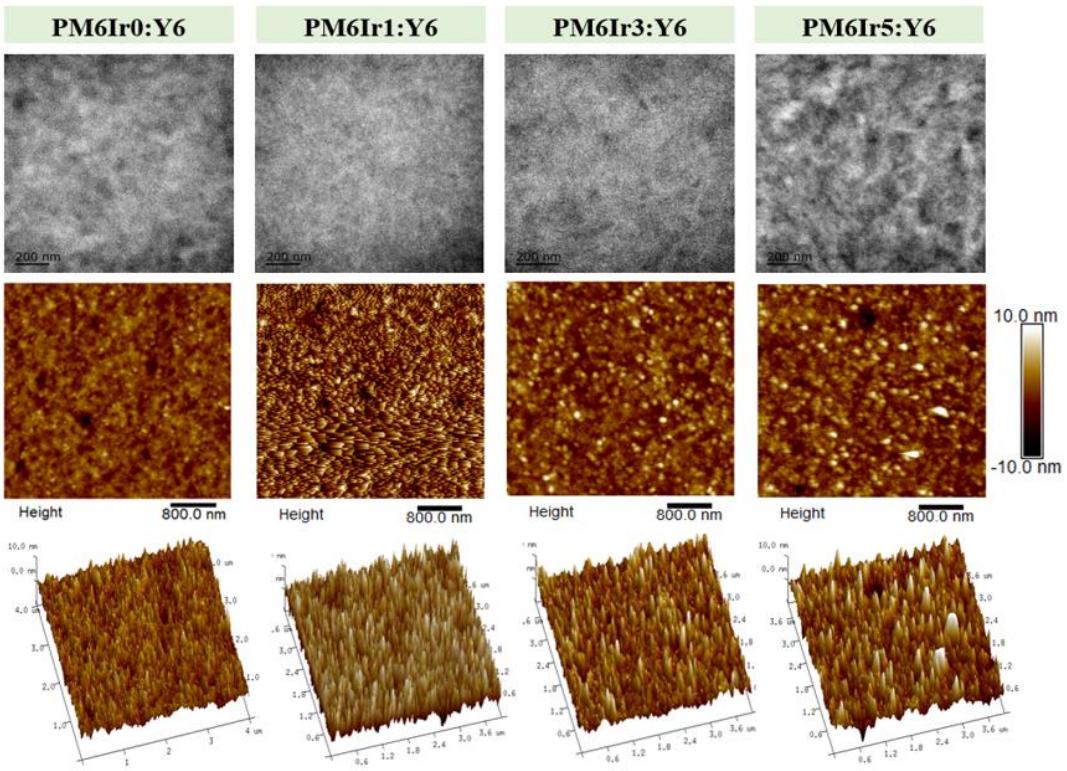

Fig. 5. TEM and AFM images of polymer:Y6 blend films.

It is generally known that the charge transport and recombination are closely related to the molecular arrangement and active layer morphology. **Fig. 5** presents the transmission electron microscope (TEM) and tapping-mode atomic force microscopy (AFM) images to investigate the effect of different M1 content on the active layer bulk and surface morphologies. In the TEM images, all blend films exhibit fine nanofibrous structure with light and dark patterns. The introduction of M1 has an obvious influence on the phase separation of the active layer. Compared with the PM6Ir0:Y6 based blend film, the phase separation is decreased due to the denser nanofibrous structures and smaller domain size for PM6Ir1:Y6 based blend film, which is in favor of the more donor/acceptor interfaces for exciton dissociation. The results are in accordance with the increased η_{diss} values from the J_{ph}-V_{eff} measurement. Then the phase separation is gradually enlarged along with the increase of M1 content, especially for the PM6Ir5:Y6

based blend film with a distinct donor aggregation. The introduction of an excess M1 content damages the miscibility between polymer donor and Y6, leading to rapidly degraded PCEs of PM6Ir5:Y6 based PSCs. According to the AFM height images with the same color bar, the root-mean-square roughness values are calculated to be 1.51 nm, 3.14 nm, 1.94 nm and 2.24 nm for PM6Ir0/PM6Ir1/PM6Ir3/PM6Ir5:Y6 based blend films, respectively. The rougher surface is formed for M1-containing blend films, especially for the optimal PM6Ir1:Y6 blend films. Meanwhile, the height distribution images exhibit some big differences between the PM6Ir1:Y6 blend film and the other three blend films (PM6Ir0:Y6, PM6Ir3:Y6 and PM6Ir5:Y6). The relatively uniform surface morphology with small grain size could be clearly observed from two- or three-dimensional AFM images of PM6Ir1:Y6 based films. This well-distributed surface morphology is beneficial to the charge collection in the active layer for getting a higher device performance [61, 62]. The TEM and AFM results illustrate the positive contribution of adding 1% M1 on optimizing the active layer bulk and surface morphology.

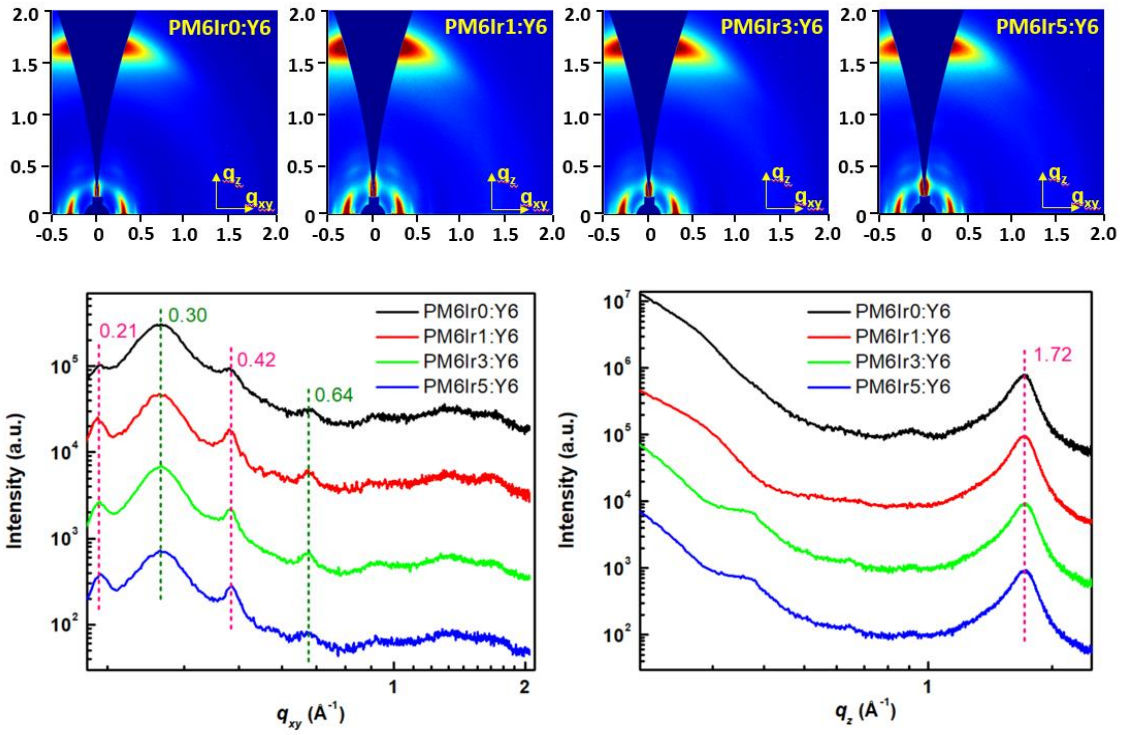

Fig. 6. 2D-GIWAXS patterns of polymer:Y6 blend films and the extracted IP and OOP line-cut profiles

of the corresponding blend films.

To further probe the molecular orientation and stacking behaviors, two-dimensional grazing incidence wide angle X-ray scattering (2D-GIWAXS) measurement was conducted on neat polymer films and polymer:Y6 blend films. As shown in **Fig. S11**, neat polymer films exhibit broad (100) diffraction peaks at ~0.30 $Å^{-1}$ along both in-plane (IP) and out-of-plane (OOP) directions, corresponding to a lamellar *d*-spacing of ~20.9 Å. Meanwhile, the (200) or (300) diffraction peaks at ~0.63 $Å^{-1}$ and ~0.90 $Å^{-1}$ are observed along the IP and OOP directions, indicating that these polymers have a relatively good crystallinity in the film state. Neat polymer films also show apparent (010) diffraction peaks at ~1.66 $Å^{-1}$ along the OOP direction, corresponding to a π–π stacking *d*-spacing of ~3.78 Å. Both edge-on and face-on orientations exist in the neat polymer films due to the relatively strong (100) and (010) diffraction peaks along the OOP direction. **Fig. 6** depicts the 2D-GIWAXS patterns and extracted line-cut profiles of the blend films along the IP and OOP directions. The diffraction peaks at ~0.30 $Å^{-1}$ along the IP direction are in accordance with that in the neat films, which should arise mainly from the polymer crystallinity in the blend films. Compared with the neat polymer films, two extra (100) diffraction peaks appear at ~0.21 $Å^{-1}$ and ~0.42 $Å^{-1}$ along the IP direction. Based on the reported work, the two diffraction peaks should be assigned to the lamellar and end-group π-π stacking of Y6 in the blend films [9, 41]. In the blend films, the (010) diffraction peaks are shifted to 1.72 $Å^{-1}$, which should originate from the synergistic crystallinity of the polymers and Y6.

By blending the polymers with Y6, the IP (010) and OOP (100) diffraction peaks almost completely disappear. The blend films exhibit a preferred face-on molecular orientation, as confirmed from the pronounced IP (100) and OOP (010) diffraction peaks. For all blend films, the positions of diffraction

peaks along the OOP and IP directions remain unchanged. Compared with the PM6Ir0:Y6 blend films, the IP (100) and OOP (010) diffraction peaks are evidently improved for PM6Ir1/PM6Ir3/PM6Ir5:Y6 blend films. The face-on molecular orientation should be increased after introducing M1 into the polymer backbone, which is beneficial to the charge transport in the vertical direction across the electrodes. The crystal coherence lengths (CCLs) of the diffraction peaks are evaluated according to the Scherrer equation: CCL = $2\pi k$/FWHM, where k is the shape factor typically with the value of 0.9, and FWHM is the full width at the half maximum. The FWHM of the diffraction peaks were obtained by the Gaussian fitting. The CCLs of the lamellar (q = 0.30 Å^{-1}) /π-π (q = 1.72 Å^{-1}) stacking are 86.9/20.6 Å, 91.2/20.4 Å, 89.0/20.0 Å and 86.4/20.0 Å for PM6Ir0/PM6Ir1/PM6Ir3/PM6Ir5:Y6 based blend films, respectively. The CCLs of the π-π stacking show a tiny change for all blend films. The CCLs of the lamellar stacking for the PM6Ir1:Y6 blend films are obviously increased, which correspond to a higher domain crystallinity in PM6Ir1 [58, 63]. It can be concluded that the molecular arrangement of polymers and Y6 can be kept in all blend films, even though a 5% M1 is introduced into the polymer backbone.

3. Conclusions

In summary, a new iridium complex, named M1, was reported and introduced into the polymer backbone of a commercial PM6 through a terpolymer strategy. Four polymers were synthesized (PM6Ir0, PM6Ir1, PM6Ir3 and PM6Ir5) and used to fabricate PSCs with Y6 as the acceptor. The PM6Ir0:Y6 based control device exhibits a PCE of 15.65% with a J_{SC} of 25.21 mA cm^{-2}, V_{OC} of 0.842 V and FF of 73.71%. The highest PCE of 16.71% is achieved for PM6Ir1:Y6 based PSCs with a J_{SC} of 26.16 mA cm^{-2}, V_{OC} of 0.848 V and FF of 75.33%. The markedly increased J_{SC} should be mainly attributed to the simultaneously improved photon harvesting and charge mobility of the active layer. The increased population and lifetime of the triplet excitons should also contribute to the J_{SC}

improvement. The optimized phase separation, molecular arrangement and uniform surface morphology are the primary factors for the increased FF of PM6Ir1:Y6 based PSCs. The PCE is sharply dropped to 14.97% for PM6Ir5:Y6 based PSCs, originating from the decreased J_{SC} of 25.09 mA cm^{-2} and FF of 70.93%. The 2D-GIWAXS measurements demonstrate that the molecular crystallinity and orientation can be kept in all blend films. The decreased PCE should be due to the serious charge recombination caused by the deteriorated phase separation, surface morphology and unbalanced charge transport. This work demonstrates that introduction of an appropriate iridium complex with strong absorption in the visible region into highly efficient polymer donors is an effective approach to improve the photovoltaic performance. New structures of triplet-based metal complexes with strong absorption in the visible or near-infrared region should be further explored for highly efficient organometallic polymer donor materials.

CRediT authorship contribution statement

M. Zhang synthesized the iridium complex M1 and four polymer donors, as well as conducted the materials/device analysis and characterization. X. Ma carried out the device fabrication and characterization. H. Zhang, L. Zhu, L. Xu helped in some material characterizations. F. Zhang contributed to the device fabrication and manuscript revision. L. Lee and C. Tsang provided the help for steady-state and transient PL measurement. H. Woo carried out the 2D-GIWAXS experiment. M. Zhang and W.-Y. Wong designed the experiments and finished the manuscript writing. F. Zhang, Z. He and W.-Y. Wong provided the support for the research resources.

Declaration of Competing Interest

The authors declare that they have no known competing financial interests or personal relationships that could have appeared to influence the work reported in this paper.

Acknowledgements

This work was supported by the Science, Technology and Innovation Committee of Shenzhen Municipality (JCYJ20180507183413211), the National Natural Science Foundation of China (52073242), the Hong Kong Research Grants Council (PolyU 153058/19P and C5037-18G), Hong Kong Polytechnic University (1-ZE1C), Research Institute for Smart Energy (CDA2), Ms. Clarea Au for the Endowed Professorship in Energy (847S), the Guangdong International Science and Technology Cooperation Foundation (2020A0505100002), Hong Kong Scholars Program (XJ2019013) and the National Natural Science Foundation of China (61975006).

Appendix A. Supplementary data

Supplementary materials to this article can be found online.

References

[1] Q. Yue, W. Liu, X. Zhu, N-type molecular photovoltaic materials: design strategies and device applications, J. Am. Chem. Soc. 142 (2020) 11613-11628.

[2] Z. Zheng, H. Yao, L. Ye, Y. Xu, S. Zhang, J. Hou, PBDB-T and its derivatives: a family of polymer donors enables over 17% efficiency in organic photovoltaics, Mater. Today 35 (2020) 115-130.

[3] Z. Hu, J. Wang, X. Ma, J. Gao, C. Xu, K. Yang, Z. Wang, J. Zhang, F. Zhang, A critical review on semitransparent organic solar cells, Nano Energy 78 (2020) 105376.

[4] Y. Lin, J. Wang, Z. Zhang, H. Bai, Y. Li, D. Zhu, X. Zhan, An electron acceptor challenging fullerenes for efficient polymer solar cells, Adv. Mater. 27 (2015) 1170-1174.

[5] S. Liu, J. Yuan, W. Deng, M. Luo, Y. Xie, Q. Liang, Y. Zou, Z. He, H. Wu, Y. Cao, High-efficiency organic solar cells with low non-radiative recombination loss and low energetic disorder, Nat. Photonics 14 (2020) 300-305.

[6] Y. Cui, H. Yao, J. Zhang, K. Xian, T. Zhang, L. Hong, Y. Wang, Y. Xu, K. Ma, C. An, C. He, Z. Wei, F. Gao, J. Hou, Single-junction organic photovoltaic cells with approaching 18% efficiency, Adv. Mater. 32 (2020) 1908205.

[7] H. Yao, Y. Cui, R. Yu, B. Gao, H. Zhang, J. Hou, Design, synthesis, and photovoltaic characterization of a small molecular acceptor with an ultra-narrow band gap, Angew. Chem. Int. Ed. 56 (2017) 3045-3049.

[8] C. Yan, S. Barlow, Z. Wang, H. Yan, A. Jen, S. Marder, X. Zhan, Non-fullerene acceptors for organic solar cells, Nat. Rev. Mater. 3 (2018) 18003.

[9] J. Yuan, Y. Zhang, L. Zhou, G. Zhang, H. Yip, T. Lau, X. Lu, C. Zhu, H. Peng, P. Johnson, M. Leclerc, Y. Cao, J. Ulanski, Y. Li, Y. Zou, Single-junction organic solar cell with over 15% efficiency using fused-ring acceptor with electron-deficient core, Joule 3 (2019) 1140-1151.

[10] M. Zhang, Z. Zhang, J. Wang, Q. An, H. Peng, W. Tang, F. Zhang, 13.26% Efficiency polymer solar cells by optimizing photogenerated exciton distribution and phase separation with the third component, Solar RRL 3 (2019) 1900269.

[11] J. Gao, J. Wang, Q. An, X. Ma, Z. Hu, C. Xu, X. Zhang, F. Zhang, Over 16.7% efficiency of ternary organic photovoltaics by employing extra $PC_{71}BM$ as morphology regulator, Sci. China Chem. 63 (2020) 83-91.

[12] Y. Tong, Z. Xiao, X. Du, C. Zuo, Y. Li, M. Lv, Y. Yuan, C. Yi, F. Hao, Y. Hua, T. Lei, Q. Lin, K. Sun, D. Zhao, C. Duan, X. Shao, W. Li, H. Yip, Z. Xiao, B. Zhang, Q. Bian, Y. Cheng, S. Liu, M. Cheng, Z. Jin, S. Yang, L. Ding, Progress of the key materials for organic solar cells, Sci. China Chem. 63 (2020) 758-765.

[13] D. Dang, D. Yu, E. Wang, Conjugated donor–acceptor terpolymers toward high-efficiency polymer solar cells, Adv. Mater. 31 (2019) 1807019.

[14] J. Du, K. Hu, L. Meng, I. Angunawela, J. Zhang, S. Qin, A. Liebman Pelaez, C. Zhu, Z. Zhang, H. Ade, Y. Li, High-performance all-polymer solar cells: synthesis of polymer acceptor by a random ternary copolymerization strategy, Angew. Chem. Int. Ed. 59 (2020) 15181-15185.

[15] Y. Cui, H. Yao, L. Hong, T. Zhang, Y. Xu, K. Xian, B. Gao, J. Qin, J. Zhang, Z. Wei, J. Hou, Achieving over 15% efficiency in organic photovoltaic cells via copolymer design, Adv. Mater. 31 (2019) 1808356.

[16] N. Kolhe, D. Tran, H. Lee, D. Kuzuhara, N. Yoshimoto, T. Koganezawa, S. Jenekhe, New random copolymer acceptors enable additive-free processing of 10.1% efficient all-polymer solar cells with near-unity internal quantum efficiency, ACS Energy Lett. 4 (2019) 1162-1170.

[17] J. Wu, G. Li, J. Fang, X. Guo, L. Zhu, B. Guo, Y. Wang, G. Zhang, L. Arunagiri, F. Liu, H. Yan, M. Zhang, Y. Li, Random terpolymer based on thiophene-thiazolothiazole unit enabling efficient non-fullerene organic solar cells, Nat. Commun. 11 (2020) 4612.

[18] H. Sun, B. Liu, C. Koh, Y. Zhang, J. Chen, Y. Wang, P. Chen, B. Tu, M. Su, H. Wang, Y. Tang, Y. Shi, H. Woo, X. Guo, Imide-functionalized heteroarene-based n-type terpolymers incorporating intramolecular noncovalent sulfur···oxygen interactions for additive-free all-polymer solar cells, Adv. Funct. Mater. 29 (2019) 1903970.

[19] H. Meng, C. Liao, M. Deng, X. Xu, L. Yu, Q. Peng, 18.77 % Efficiency organic solar cells promoted by aqueous solution processed cobalt(II) acetate hole transporting layer, Angew. Chem. Int. Ed. (2021) DOI: org/10.1002/ange.202110550.

[20] J. Song, L. Zhu, C. Li, J. Xu, H. Wu, X. Zhang, Y. Zhang, Z. Tang, F. Liu, Y. Sun, High-efficiency organic solar cells with low voltage loss induced by solvent additive strategy, Matter 4 (2021) 2542-2552.

[21] S. Chen, L. Feng, T. Jia, J. Jing, Z. Hu, K. Zhang, F. Huang, High-performance polymer solar cells with efficiency over 18% enabled by asymmetric side chain engineering of non-fullerene acceptors, Sci. China Chem. 64 (2021) 1192-1199.

[22] C. Li, J. Zhou, J. Song, J. Xu, H. Zhang, X. Zhang, J. Guo, L. Zhu, D. Wei, G. Han, J. Min, Y. Zhang, Z. Xie, Y. Yi, H. Yan, F. Gao, F. Liu, Y. Sun, Non-fullerene acceptors with branched side chains and improved molecular packing to exceed 18% efficiency in organic solar cells, Nat. Energy 6 (2021) 605-613.

[23] Q. Liu, Y. Jiang, K. Jin, J. Qin, J. Xu, W. Li, J. Xiong, J. Liu, Z. Xiao, K. Sun, S. Yang, X. Zhang, L. Ding, 18% Efficiency organic solar cells, Sci. Bull. 65 (2020) 272-275.

[24] L. Xu, C. Ho, L. Liu, W. Wong, Molecular/polymeric metallaynes and related molecules: solar cell materials and devices, Coord. Chem. Rev. 373 (2018) 233-257.

[25] C. Ho, Z. Yu, W. Wong, Multifunctional polymetallaynes: properties, functions and applications, Chem. Soc. Rev. 45 (2016) 5264-5295.

[26] Y. Jin, Y. Zhang, Y. Liu, J. Xue, W. Li, J. Qiao, F. Zhang, Limitations and perspectives on triplet-material-based organic photovoltaic devices, Adv. Mater. 31 (2019) 1900690.

[27] A. Heeger, 25th Anniversary article: bulk heterojunction solar cells: understanding the mechanism

of operation, Adv. Mater. 26 (2014) 10-28.

[28] L. Yang, W. Gu, L. Lv, Y. Chen, Y. Yang, P. Ye, J. Wu, L. Hong, A. Peng, H. Huang, Triplet tellurophene-based acceptors for organic solar cells, Angew. Chem. Int. Ed. 57 (2018) 1096-1102.

[29] L. Qin, X. Liu, X. Zhang, J. Yu, L. Yang, F. Zhao, M. Huang, K. Wang, X. Wu, Y. Li, H. Chen, K. Wang, J. Xia, X. Lu, F. Gao, Y. Yi, H. Huang, Triplet acceptors with a D-A structure and twisted conformation for efficient organic solar cells, Angew. Chem. Int. Ed. 59 (2020) 15043-15049.

[30] M. Qian, R. Zhang, J. Hao, W. Zhang, Q. Zhang, J. Wang, Y. Tao, S. Chen, J. Fang, W. Huang, Dramatic enhancement of power conversion efficiency in polymer solar cells by conjugating very low ratio of triplet iridium complexes to PTB7, Adv. Mater. 27 (2015) 3546-3552.

[31] T. Wang, R. Sun, M. Shi, F. Pan, Z. Hu, F. Huang, Y. Li, J. Min, Solution-processed polymer solar cells with over 17% efficiency enabled by an iridium complexation approach, Adv. Energy Mater. 10 (2020) 2000590.

[32] Z. Wan, J. Yang, Y. Liu, S. Wang, Y. Zhong, C. Li, Z. Zhang, G. Xing, S. Huettner, Y. Tao, Y. Li, W. Huang, Cyclometalated Pt complex-based random terpolymers for efficient polymer solar cells, Poly. Chem. 8 (2017) 4729-4737.

[33] X. Xu, K. Feng, Z. Bi, W. Ma, G. Zhang, Q. Peng, Single-junction polymer solar cells with 16.35% efficiency enabled by a platinum(II) complexation strategy, Adv. Mater. 31 (2019) 1901872.

[34] T. Liu, R. Ma, Z. Luo, Y. Guo, G. Zhang, Y. Xiao, T. Yang, Y. Chen, G. Li, Y. Yi, X. Lu, H. Yan, B. Tang, Concurrent improvement in J_{SC} and V_{OC} in high-efficiency ternary organic solar cells enabled by a red-absorbing small-molecule acceptor with a high LUMO level, Energy Environ. Sci. 13 (2020) 2115-2123.

[35] Y. Ma, D. Cai, S. Wan, P. Yin, P. Wang, W. Lin, Q. Zheng, Control over π-π stacking of

heteroheptacene-based nonfullerene acceptors for 16% efficiency polymer solar cells, Nat. Sci. Rev. 7 (2020) 1886-1895.

[36] M. Zhang, X. Guo, W. Ma, H. Ade, J. Hou, A large-bandgap conjugated polymer for versatile photovoltaic applications with high performance, Adv. Mater. 27 (2015) 4655-4660.

[37] M. Zhang, J. Wang, X. Ma, J. Gao, C. Xu, Z. Hu, L. Niu, F. Zhang, Review on smart strategies for achieving highly efficient ternary polymer solar cells, APL Mater. 8 (2020) 090703.

[38] T. Yan, W. Song, J. Huang, R. Peng, L. Huang, Z. Ge, 16.67% Rigid and 14.06% flexible organic solar cells enabled by ternary heterojunction strategy, Adv. Mater. 31 (2019) 1902210.

[39] J. Song, C. Li, L. Zhu, J. Guo, J. Xu, X. Zhang, K. Weng, K. Zhang, J. Min, X. Hao, Y. Zhang, F. Liu, Y. Sun, Ternary organic solar cells with efficiency >16.5% based on two compatible nonfullerene acceptors, Adv. Mater. 31 (2019) 1905645.

[40] S. Dong, T. Jia, K. Zhang, J. h. Jing, F. Huang, Single-component non-halogen solvent-processed high-performance organic solar cell module with efficiency over 14%, Joule 4 (2020) 2004-2016.

[41] T. Shan, Y. Zhang, Y. Wang, Z. Xie, Q. Wei, J. Xu, M. Zhang, C. Wang, Q. Bao, X. Wang, C. Chen, J. Huang, Q. Chen, F. Liu, L. Chen, H. Zhong, Universal and versatile morphology engineering via hot fluorous solvent soaking for organic bulk heterojunction, Nat. Commun. 11 (2020) 5585.

[42] C. Xu, H. Chen, Z. Zhao, J. Gao, X. Ma, S. Lu, X. Zhang, Z. Xiao, F. Zhang, 14.46% Efficiency small molecule organic photovoltaics enabled by the well trade-off between phase separation and photon harvesting, J. Energy Chem. 57 (2021) 610-617.

[43] X. Wang, Q. Sun, J. Gao, X. Ma, J. Son, S. Jeong, Z. Hu, L. Niu, H. Woo, J. Zhang, F. Zhang, Ternary organic photovoltaic cells exhibiting 17.59% efficiency with two compatible Y6 derivations as acceptor, Solar RRL 5 (2021) 2100007.

[44] M. Zhang, Z. Xiao, W. Gao, Q. Liu, K. Jin, W. Wang, Y. Mi, Q. An, X. Ma, X. Liu, C. Yang, L. Ding, F. Zhang, Over 13% efficiency ternary nonfullerene polymer solar cells with tilted up absorption edge by incorporating a medium bandgap acceptor, Adv. Energy Mater. 8 (2018) 1801968.

[45] G. Chai, Y. Chang, Z. Peng, Y. Jia, X. Zou, D. Yu, H. Yu, Y. Chen, P. Y. Chow, K. Wong, J. Zhang, H. Ade, L. Yang, C. Zhan, Enhanced hindrance from phenyl outer side chains on nonfullerene acceptor enables unprecedented simultaneous enhancement in organic solar cell performances with 16.7% efficiency, Nano Energy 76 (2020) 105087.

[46] M. Zhang, W. Gao, F. Zhang, Y. Mi, W. Wang, Q. An, J. Wang, X. Ma, J. Miao, Z. Hu, X. Liu, J. Zhang, C. Yang, Efficient ternary non-fullerene polymer solar cells with PCE of 11.92% and FF of 76.5%, Energy Environ. Sci. 11 (2018) 841-849.

[47] Q. An, J. Wang, X. Ma, J. Gao, Z. Hu, B. Liu, H. Sun, X. Guo, X. Zhang, F. Zhang, Two compatible polymer donors contribute synergistically for ternary organic solar cells with 17.53% efficiency, Energy Environ. Sci. 13 (2020) 5039-5047.

[48] L. Nian, Y. Kan, H. Wang, K. Gao, B. Xu, Q. Rong, R. Wang, J. Wang, F. Liu, J. Chen, G. Zhou, T. Russell, A. Jen, Ternary non-fullerene polymer solar cells with 13.51% efficiency and a record-high fill factor of 78.13%, Energy Environ. Sci. 11 (2018) 3392-3399.

[49] X. Xu, L. Yu, H. Yan, R. Li, Q. Peng, Highly efficient non-fullerene organic solar cells enabled by a delayed processing method using a non-halogenated solvent, Energy Environ. Sci. 13 (2020) 4381-4388.

[50] Q. An, J. Wang, W. Gao, X. Ma, Z. Hu, J. Gao, C. Xu, M. Hao, X. Zhang, C. Yang, F. Zhang, Alloy-like ternary polymer solar cells with over 17.2% efficiency, Sci. Bull. 65 (2020) 538-545.

[51] L. Meng, Y. Zhang, X. Wan, C. Li, X. Zhang, Y. Wang, X. Ke, Z. Xiao, L. Ding, R. Xia, H. Yip, Y. Cao, Y. Chen, Organic and solution-processed tandem solar cells with 17.3% efficiency, Science 361 (2018) 1094.

[52] H. Sun, H. Yu, Y. Shi, J. Yu, Z. Peng, X. Zhang, B. Liu, J. Wang, R. Singh, J. Lee, Y. Li, Z. Wei, Q. Liao, Z. Kan, L. Ye, H. Yan, F. Gao, X. Guo, A narrow-bandgap n-type polymer with an acceptor-acceptor backbone enabling efficient all-polymer solar cells, Adv. Mater. 32 (2020) 2004183.

[53] X. Yang, H. Guo, B. Liu, J. Zhao, G. Zhou, Z. Wu, W. Wong, Diarylboron-based asymmetric red-emitting Ir(III) complex for solution-processed phosphorescent organic light-emitting diode with external quantum efficiency above 28%, Adv. Sci. 5 (2018) 1701067.

[54] Z. Chen, L. Wang, C. Ho, S. Chen, S. Suramitr, A. Plucksacholatarn, N. Zhu, S. Hannongbua, W. Wong, Smart design on the cyclometalated ligands of iridium(III) complexes for facile tuning of phosphorescence color spanning from deep-blue to near-infrared, Adv. Opt. Mater. 6 (2018) 1800824.

[55] J. Seo, N. Han, H. Shim, S. Park, J. Kwon, J. Song, Triplet state and phosphorescence of hole-transport layer and its triplet exciton confinement, Chem. Phys. Lett. 499 (2010) 226-230.

[56] L. Perdigon-Toro, H. Zhang, A. Markina, J. Yuan, S. Hosseini, C. Wolff, G. Zuo, M. Stolterfoht, Y. Zou, F. Gao, D. Andrienko, S. Shoaee, D. Neher, Barrierless free charge generation in the high-performance PM6:Y6 bulk heterojunction non-fullerene solar cell, Adv. Mater. 32 (2020) 1906763.

[57] S. Pang, Z. Wang, X. Yuan, L. Pan, W. Deng, H. Tang, H. Wu, S. Chen, C. Duan, F. Huang, Y. Cao, A facile synthesized polymer featuring B-N covalent bond and small singlet-triplet gap for high-performance organic solar cells, Angew. Chem. Int. Edit. 60 (2021) 8813-8817.

[58] X. Ma, A. Zeng, J. Gao, Z. Hu, C. Xu, J. Son, S. Jeong, C. Zhang, M. Li, K. Wang, H. Yan, Z. Ma,

Y. Wang, H. Woo, F. Zhang, Approaching 18% efficiency of ternary organic photovoltaics with wide bandgap polymer donor and well compatible Y6:Y6-1O as acceptor, Nat. Sci. Rev. (2021) nwaa305.

[59] L. Zhu, M. Zhang, G. Zhou, T. Hao, J. Xu, J. Wang, C. Qiu, N. Prine, J. Ali, W. Feng, X. Gu, Z. Ma, Z. Tang, H. Zhu, L. Ying, Y. Zhang, F. Liu, Efficient organic solar cell with 16.88% efficiency enabled by refined acceptor crystallization and morphology with improved charge transfer and transport properties, Adv. Energy Mater. 10 (2020) 1904234.

[60] X. Zhang, L. Qin, X. Liu, C. Zhang, J. Yu, Z. Xiao, N. Zheng, B. Wang, Y. Wei, Z. Xie, Y. Wu, Z. Wei, K. Wang, F. Gao, L. Ding, H. Huang, Enhancing the photovoltaic performance of triplet acceptors enabled by side-chain engineering, Solar RRL (2021) 2100522.

[61] M. Zhang, R. Ming, W. Gao, Q. An, X. Ma, Z. Hu, C. Yang, F. Zhang, Ternary polymer solar cells with alloyed non-fullerene acceptor exhibiting 12.99% efficiency and 76.03% fill factor, Nano Energy 59 (2019) 58-65.

[62] J. Gao, J. Wang, C. Xu, Z. Hu, X. Ma, X. Zhang, L. Niu, J. Zhang, F. Zhang, A critical review on efficient thick-film organic solar cells, Solar RRL 4 (2020) 2000364.

[63] C. Yan, H. Tang, R. Ma, M. Zhang, T. Liu, J. Lv, J. Huang, Y. Yang, T. Xu, Z. Kan, H. Yan, F. Liu, S. Lu, G. Li, Synergy of liquid-crystalline small-molecule and polymeric donors delivers uncommon morphology evolution and 16.6% efficiency organic photovoltaics, Adv. Sci. 7 (2020) 2000149.